AIAA Meeting Papers on Disc, January 1996
A9618387, N00014-93-1-0342, AIAA Paper 96-0425

High Reynolds number flow simulations using the localized dynamic subgrid-scale model

S. Menon
Georgia Inst. of Technology, Atlanta

W.-W. Kim
Georgia Inst. of Technology, Atlanta

AIAA 34th Aerospace Sciences Meeting and Exhibit, Reno, NV Jan 15-18, 1996

The localized dynamic subgrid-scale model introduced by Kim and Menon (1995) has been used in large-eddy simulations of decaying and forced isotropic turbulence and temporally evolving turbulent mixing layer for high Reynolds numbers. In the simulations of isotropic turbulence, it is demonstrated that the low-resolution large-eddy simulation results accurately reproduce the characteristics of a realistic, high-Reynolds number turbulence such as the power-law decay (decaying case), and the velocity statistics and the development of the non-Gaussian statistics (forced case). From the large-eddy simulations of temporally evolving turbulent mixing layer, the time-accurate results, which agree very well with the existing high-resolution direct numerical simulation and experimental data, are obtained using a new scaling which is capable of separating the distinct effects of initial development on the self-similar stage of the mixing layer evolution. (Author)

AIAA-96-0425

HIGH REYNOLDS NUMBER FLOW SIMULATIONS USING THE LOCALIZED DYNAMIC SUBGRID-SCALE MODEL

Suresh Menon*and Won-Wook Kim†
School of Aerospace Engineering
Georgia Institute of Technology
Atlanta, Georgia

ABSTRACT

The localized dynamic subgrid-scale model introduced by Kim & Menon (1995), has been used in large-eddy simulations of decaying and forced isotropic turbulence, and temporally evolving turbulent mixing layer for high Reynolds numbers. In the simulations of isotropic turbulence, it is demonstrated that the low-resolution large-eddy simulation results accurately reproduce the characteristics of a realistic, high-Reynolds number turbulence such as the power-law decay (decaying case), and the velocity statistics and the development of the non-Gaussian statistics (forced case). From the large-eddy simulations of temporally evolving turbulent mixing layer, the time-accurate results, which agree very well with the existing high-resolution direct numerical simulation and experimental data, are obtained using a new scaling which is capable of separating the distinct effects of initial development on the self-similar stage of the mixing layer evolution.

1 INTRODUCTION

The dynamic subgrid-scale (SGS) model, introduced by Germano *et al.* (1991), has been successfully applied to various types of flow fields (Moin *et al.*, 1991; Piomelli, 1993; Squires & Piomelli, 1994; Ghosal *et al.*, 1995). Two desirable features make this model especially attractive. First, the model coefficient is determined as a part of the solution, thus, removing the major limitation of the conventional eddy-viscosity type SGS models which was the inability to parameterize accurately the unresolved SGS stresses in different turbulent flows with a single *universal* constant. Second, as a result of the dynamic determination, the model coefficient can become negative in certain regions of the flow field and, thus, appears to have the capability to mimic backscatter of energy from the subgrid-scales to the resolved scales. Although it has been shown that Germano *et al.*'s dynamic model is superior to the conventional fixed-coefficient model, the dynamic procedure, as developed earlier, still has some deficiencies. These deficiencies originate from a weakness of the Smagorinsky model used in Germano *et al.*'s dynamic model, as well as, from the mathematically inconsistent derivation and the ill-conditioning of the dynamic formulation itself.

Recently, Kim and Menon (1995a,b) developed a new localized dynamic subgrid-scale (LDKSGS) model associated with the SGS kinetic energy equation model. In this model, all deficiencies of Germano *et al.*'s dynamic subgrid-scale model were overcome. This model also provides a straightforward localized evaluation of the model coefficients which do not cause any numerical instability. Moreover, the localized model coefficients obtained from this model are proved to be Galilean-invariant and very realizable. The localized dynamic model was applied to Taylor-Green vortex flows and, it was shown that this model predicts the turbulent flow field more accurately than the previously developed dynamic models. In this paper, the application of this model to high Reynolds number decaying and forced isotropic turbulence, and turbulent mixing layers is discussed. The results are compared with predictions using experiments, direct numerical simulation (DNS) and large-eddy simulations (LES) using Germano *et al.*'s dynamic model.

The numerical simulations were carried out using a finite-difference code that is second-order accurate in time and fifth-order (the convective terms) and sixth-order (the viscous terms) accurate in space using upwind-biased differences. Time-accurate solutions of the incompressible Navier-Stokes equations are obtained by the artificial compressibility approach which requires subiteration in pseudotime to get the

*Associate Professor, Senior Member AIAA.
†Graduate Research Assistant, Student Member AIAA.

divergence-free flow field. A significant acceleration of the convergence to a steady-state divergence-free solution in pseudotime is achieved by incorporating the full approximation scheme (FAS) multigrid method. Earlier (Menon and Yeung, 1994), this code was validated by carrying out DNS of decaying isotropic turbulence and comparing the resulting statistics with the predictions of a well known psuedo spectral code. Further validation of this code is demonstrated in this study by comparison with experiments.

In section 2, the LDKSGS model is described with the basic equations indicating its advantages. In section 3, the LDKSGS model is applied to decaying and force isotropic turbulence, and temporally evolving turbulent mixing layer. Conclusions are presented in section 4.

2 Localized dynamic k-equation SGS (LDKSGS) model

In physical space, the incompressible Navier-Stokes equations for LES are obtained by filtering them using low-pass filter of a computational mesh (hence, the characteristic length of this filter is the grid width $\overline{\Delta}$) as follows,

$$\frac{\partial \overline{u}_i}{\partial x_i} = 0 \tag{1}$$

$$\frac{\partial \overline{u}_i}{\partial t} + \overline{u}_j \frac{\partial \overline{u}_i}{\partial x_j} = -\frac{\partial}{\partial x_j}\left(\overline{p}\delta_{ij} + \tau_{ij}\right) + \nu \frac{\partial^2 \overline{u}_i}{\partial x_j \partial x_j} \tag{2}$$

where $\overline{u}_i(x_i,t)$ is the resolved velocity field. The application of the grid filter results in the following unknown SGS stress tensor, $\tau_{ij} = \overline{u_i u_j} - \overline{u}_i \overline{u}_j$, which needs to be modeled in terms of the resolved velocity field $\overline{u}$. Eddy viscosity assumption implies $\tau_{ij} = -2\nu_T \overline{S}_{ij} + \frac{1}{3}\delta_{ij}\tau_{kk}$ where ν_T is the eddy viscosity and $\overline{S}_{ij} = \frac{1}{2}\left(\partial \overline{u}_i/\partial x_j + \partial \overline{u}_j/\partial x_i\right)$. Simple dimensional arguments suggest that the eddy viscosity ν_T should be given by the product of a velocity scale and a length scale. In LES, the length scale is usually related to the filter size ($\overline{\Delta}$), however, models differ in their prescription for the velocity scale which can be estimated from the smallest resolved scales. In the Smagorinsky model, an algebraically described velocity scale is obtained by assuming that an equilibrium exists between energy production and dissipation in the small scales. One-equation SGS model solves the following transport equation (e.g. Menon *et al.*, 1995) for the subgrid-scale kinetic energy, $k_{sgs} = \frac{1}{2}\left(\overline{u_i u_i} - \overline{u}_i \overline{u}_i\right)$, to provide the velocity scale:

$$\frac{\partial k_{sgs}}{\partial t} + \overline{u}_i \frac{\partial k_{sgs}}{\partial x_i} = -\tau_{ij}\frac{\partial \overline{u}_i}{\partial x_j} - \varepsilon + \frac{\partial}{\partial x_i}\left(\nu_T \frac{\partial k_{sgs}}{\partial x_i}\right) \tag{3}$$

Here, the three terms on the right-hand-side of (3) represent, respectively, the production, dissipation and diffusion of k_{sgs}. In the model of the diffusion term, the direct effect of ν has been dropped. In the original model of this term, ν_T/σ_k is used in place of ν_T. However, since $\sigma_k = 1$ is usually adopted (Yoshizawa, 1993), σ_k has been dropped from (3). The dynamic procedure can be used to determine σ_k as described in Kim & Menon (1995b). The SGS stress tensor τ_{ij} is parameterized according to the eddy viscosity assumption and the SGS eddy viscosity ν_T is modeled as: $\nu_T = C_\tau k_{sgs}^{1/2}\overline{\Delta}$ where C_τ is an adjustable coefficient that is determined dynamically, as shown below. Equation (3) is closed by providing a model for the dissipation rate term, ε. Using simple scaling arguments, ε is usually modeled as: $\varepsilon = C_\varepsilon \overline{\Delta}^{-1} k_{sgs}^{3/2}$ where, C_ε is another coefficient that is also obtained dynamically.

To obtain the coefficients C_τ and C_ε dynamically, a top-hat test filter characterized by $\widehat{\Delta}$ (typically, $\widehat{\Delta} = 2\overline{\Delta}$) is used (the application of the test filter on any variable ϕ will be denoted by $\widehat{\phi}$). The dynamic modeling procedure employed in the present study is based on the existence of the similarity between the SGS stress $\tau_{ij} = \overline{u_i u_j} - \overline{u}_i \overline{u}_j$ and the following resolved stress $T_{ij} = \widehat{\overline{u}_i \overline{u}_j} - \widehat{\overline{u}}_i \widehat{\overline{u}}_j$ which was observed in Liu *et al.*'s (1994) analysis of experimental data in the far field of a round jet at a reasonably high Reynolds number ($Re_\lambda \approx 310$). Using the existence of the similarity, the model for τ_{ij} can be extended to T_{ij} as follows,

$$\begin{aligned} T_{ij} = \quad & -2C_\tau \widehat{\Delta}\left[\frac{1}{2}\left(\widehat{\overline{u}_i \overline{u}_i} - \widehat{\overline{u}}_i \widehat{\overline{u}}_i\right)\right]^{1/2} \widehat{\overline{S}}_{ij} \\ & + \frac{2}{3}\delta_{ij}\left[\frac{1}{2}\left(\widehat{\overline{u}_i \overline{u}_i} - \widehat{\overline{u}}_i \widehat{\overline{u}}_i\right)\right] \end{aligned} \tag{4}$$

Also, the dissipation rate at the test filter level can be modeled in a similar manner:

$$\begin{aligned} E &= (\nu + \nu_T)\left(\widehat{\frac{\partial \overline{u}_i}{\partial x_j}}\frac{\partial \overline{u}_i}{\partial x_j} - \frac{\partial \widehat{\overline{u}}_i}{\partial x_j}\frac{\partial \widehat{\overline{u}}_i}{\partial x_j}\right) \\ &= \frac{C_\varepsilon}{\widehat{\Delta}}\left[\frac{1}{2}\left(\widehat{\overline{u}_i \overline{u}_i} - \widehat{\overline{u}}_i \widehat{\overline{u}}_i\right)\right]^{3/2} \end{aligned} \tag{5}$$

Here, $(\nu + \nu_T)$ is used for E since E is described only by the resolved-range scales, while the definition of

the actual dissipation ε includes the unresolved scale information $\overline{(\partial u_i/\partial x_j)^2}$. That is, the test filter level energy, $K = \frac{1}{2}\left(\widehat{\overline{u}_i\overline{u}_i} - \widehat{\overline{u}}_i\widehat{\overline{u}}_i\right)$, is dissipated due to the SGS eddy viscosity as well as the molecular viscosity. Therefore, the effective viscosity for E is $(\nu + \nu_T)$. Now, C_τ and C_ε can be determined directly from (4) and (5). Equation (4) is a set of five independent equations for one unknown C_τ. To minimize the error that can occur solving this over-determined system, Lilly (1992) proposed a least-square method which yields

$$C_\tau = \frac{1}{2} T_{ij}\sigma_{ij}\left(\sigma_{ij}\sigma_{ij}\right)^{-1} \tag{6}$$

where

$$\sigma_{ij} = -\widehat{\Delta}\left[\frac{1}{2}\left(\widehat{\overline{u}_i\overline{u}_i} - \widehat{\overline{u}}_i\widehat{\overline{u}}_i\right)\right]^{1/2}\widehat{\overline{S}}_{ij} \tag{7}$$

Equation (5) is a scalar equation for a single unknown and, hence, an exact value C_ε can be obtained without applying any approximation:

$$C_\varepsilon = \widehat{\Delta}\left[\frac{1}{2}\left(\widehat{\overline{u}_i\overline{u}_i} - \widehat{\overline{u}}_i\widehat{\overline{u}}_i\right)\right]^{-3/2} E \tag{8}$$

As shown above, a mathematically consistent procedure is employed in this dynamic formulation (Germano *et al.*'s dynamic model formulation contains a mathematical inconsistency since the model coefficient is taken out of the spatial-filtering operation in spite of its large spatial variation). Furthermore, the denominators of the expressions for C_τ and C_ε contain the energy information within the resolved scale range which is well-defined (in Germano *et al.*'s dynamic model, the denominator in the final equation for the model coefficient contains algebraically manipulated terms that can be very small causing numerical instability and hence, the resulting expressions are ill-conditioned). Therefore, the ill-conditioning problem is not considered serious here. Also, the direct evaluation of the SGS kinetic energy prevents the prolonged occurrence of negative model coefficient which has been known to cause numerical instability in Germano *et al.*'s dynamic model. These properties of the current model enable a stable localized evaluation of the model coefficients without employing any spatial or temporal averaging. Further, note that, the expression for C_ε does not have the unphysical property of vanishing at high Reynolds numbers since the effective viscosity $(\nu + \nu_T)$ is used instead of just ν. Kim and Menon (1995b) showed that the LDKSGS model is properly Galilean-invariant and, therefore, the resulting LES equations of motion for the large eddies using the LDKSGS model retain the same form in all inertial frames of reference. They also proved that the model satisfies the realizability conditions given by the inequalities $\tau_{ii} \geq 0$ and $\tau_{ij}^2 \leq \tau_{ii}\tau_{jj}$ (Vreman *et al.*, 1994a). These ineqaulities provide the following realizable range for the dynamically determined model coefficient C_τ,

$$\frac{k_{sgs}^{1/2}}{3\overline{\Delta}\,\overline{S}_{nn}} \leq C_\tau \leq \frac{k_{sgs}^{1/2}}{3\overline{\Delta}\,\overline{S}_{ll}} \tag{9}$$

$$-\frac{2}{\sqrt{3}}\frac{k_{sgs}^{1/2}}{\overline{\Delta}\,|\overline{S}|} \leq C_\tau \leq \frac{2}{\sqrt{3}}\frac{k_{sgs}^{1/2}}{\overline{\Delta}\,|\overline{S}|} \tag{10}$$

where $\overline{S}_{ll}$ and $\overline{S}_{nn}$ denote, respectively, the largest and smallest eigenvalues of the strain rate tensor (i.e., $\overline{S}_{ll} \geq 0$ and $\overline{S}_{nn} \leq 0$ in the incompressible case). Numerical experiments using decaying isotropic turbulence (the detailed description of this flow field will be presented in the section 3.1) show that more than 99.9% (for the 48^3 grid resolution), 99.8% (for the 32^3 grid resolution), and 99.6% (for the 24^3 grid resolution) of the grid points satisfy both the realizability conditions, (9) and (10), at the same time during the entire simulation. Therefore, the LDKSGS model satisfies the realizability conditions in a more strict sense when compared to Ghosal *et al.* (1995) who reported that the DLM(k) model (which is the only other existing localized dynamic model formulated without employing the *ad hoc* averaging procedure) satisfies the realizability condition at about 95% of the grid points for the simulation of decaying isotropic turbulence using a 48^3 grid resolution. Furthermore, to examine the realizability, they used only the condition (9). According to our numerical experiments, the satisfaction of the condition (9) does not automatically guarantee the satisfaction of the condition (10). For definite realizability, both conditions, (9) and (10), should be used for accurate verification.

3 Results and Discussion

The LDKSGS model has been applied to decaying (section 3.1) and forced (section 3.2) isotropic turbulence, and turbulent mixing layer (section 3.3).

3.1 Decaying isotropic turbulence

The experiment of decaying isotropic turbulence of Comte-Bellot and Corsin (1971) is simulated to demonstrate the capability of the LDKSGS model in predicting the decay of the turbulent energy. First, the grid resolutions for possible DNS and LES are investigated by computing the resolved energy at each grid resolution (i.e., by numerically integrating the

spectrum given by Comte-Bellot & Corsin(1971) between wavenumbers zero to the maximum wavenumber resolved by the grid resolution). The results show that 384^3, 192^3, 96^3, 48^3, 32^3 and 24^3 grid resolutions resolve 99.5%, 96.6%, 87.3%, 70.3%, 59.3% and 49.7% of the total turbulent kinetic energy, respectively. Therefore, to accurately resolve all excited turbulence scales without employing any turbulence models, at least 384^3 grid resolution is needed. Also, for LES, the grid resolution used must be consistent with the basic assumption of LES that the resolved scales contains most of the energy. For this same problem, Ghosal *et al.* (1995) concluded that the 48^3 grid resolution is the smallest possible resolution for LES since, at the grid resolution coarser than 48^3, a significant number of energy-containing eddies resides in the unresolved scales and, hence, the results are greatly dependent on the quality of the SGS model employed. That is, the simulation of this experiment especially using the grid resolution coarser than 48^3 (i.e., when the subgrid scales contain more than 30% of total turbulent kinetic energy) is a good test case to measure the quality of the SGS model. For this purpose, three grid resolutions (48^3, 32^3, and 24^3) are used for the large-eddy simulations implemented here.

In the experiment, measurements of the energy spectra were carried out at three locations downstream of the mesh (which generated the turbulence in the wind tunnel). At the first measuring station, the Reynolds number based on the Taylor microscale and based on the integral scale were, respectively, 71.6 and 187.9 (these values decreased to 60.7 and 135.7, respectively, at the last measuring station). Using the assumption of a constant mean velocity across the cross section of the wind tunnel, the elapsed time for the turbulent field traveling at the mean velocity from the mesh (that is, proportional to the downstream distance) can be obtained. Therefore, this (spatially evolving) problem can be thought of as a decaying isotropic turbulence inside a cubical box which is moving with the mean flow velocity. The size of the box is chosen to be greater than the integral scale of the measured real turbulence. The statistical properties of turbulence inside the box are believed to be realistic even after applying periodic boundary condition for numerical implementation. All experimental data is nondimensionalized by the reference length scale $10M/2\pi$ (where $M = 5.08cm$ is the wind-tunnel mesh spacing) and the reference time scale 0.1 *sec* for computational convenience. (By this nondimensionalization, the three measuring locations correspond to the three dimensionless time levels, t^* =2.13, 4.98 and 8.69, respectively.)

The initial velocity field (primarily the amplitudes of the velocity Fourier modes) is chosen to match the three-dimensional energy spectrum obtained at the first experimental measuring station. The phases of Fourier modes are chosen to be random so that the initial velocity field satisfy Gaussian statistics. The initial pressure is assumed to be uniform throughout the flow field and the initial SGS kinetic energy is estimated by assuming the similarity between the SGS kinetic energy and the resolved energy at the test filter level: $k_{sgs} \approx \frac{C_K}{2}\left(\widehat{\overline{u}_i\overline{u}_i} - \widehat{\overline{u}}_i\widehat{\overline{u}}_i\right)$ where a constant C_K is determined by matching the magnitude of the SGS kinetic energy to the exact SGS kinetic energy calculated by integrating the experimental spectrum at the first measuring station. In situations where the information about the magnitude of the exact SGS kinetic energy is not known, a value of C_K can be determined by adopting the similarity concept used in the dynamic procedure. This formulation is presented in Kim & Menon (1995b).

Figure 1 shows the decay of the resolved turbulent kinetic energy computed using the LDKSGS model at three grid resolutions, 48^3, 32^3, and 24^3. The results are compared with the predictions of the volume-averaged Germano *et al.*'s model at the 48^3 grid resolution and the experimental data of Comte-Bellot and Corsin (1971). The predictions of both models (at the 48^3 grid resolution) are in good agreement with the experiment. As is well known, the turbulent kinetic energy undergoes a power law decay, i.e., $E \sim (t^*)^n$, in the asymptotic self-similar regime. The experimental data roughly confirms the existence of the power law by lying on a straight line on a log-log plot. The decay exponent n is obtained from a least-square fit to each data: -1.17 (48^3), -1.13 (32^3), and -1.09(24^3) from the LDKSGS results and -1.20 (48^3), -1.16 (32^3), and -1.12(24^3) from the experimental data. These results confirm the agreement between the predictions of LES and the experiment. More importantly, the results of the LDKSGS model at all three grid resolutions used (even for the 24^3 grid resolution where about a half of the turbulent kinetic energy is not resolved) show consistency in predicting the energy decay. This property of the model is a fascinating feature especially when the model is (to be) applied to complex and high Reynolds number flows where a significant amount of turbulent energy possibly lies in the unresolved scales. Without a self-consistent behavior, the SGS model can not simulate high Reynolds number flows in complex geometries reliably. Therefore, the proposed LDKSGS model seems to have a promising potential for application

to complex, high-Reynolds number flows.

The computed and experimental three-dimensional energy spectra resolved at the three different grid resolutions, 48^3, 32^3, and 24^3, are shown in figures 2(a) at $t^* = 4.98$ and (b) at $t^* = 8.69$. Both of the LDKSGS and volume-averaged Germano *et al*'s models predict the spectra reasonably well. Especially, the LDKSGS model predicts the spectra consistently well for all three grid resolutions. Some discrepancy between the experimental and LES-predicted energy spectra is observed around the cut-off wavenumber. This discrepancy is due to the fact that, for its discretized numerical implementation, the finite-difference code used in this study implicitly adopts the top-hat filter which yields a significant contribution to the subgrid-scale energy from the lower wavenumbers than the cut-off wavenumber (when the Fourier cut-off filter is employed, the subgrid-scale energy is entirely due to the energy in the wave numbers larger than the cut-off wavenumber). Direct comparison between experimental and LES-predicted energy spectra is meaningful only when the full-resolution experimental flow field is filtered down to the LES grid resolution to compare using the top-hat filter (to be more consistent, the initial flow field for LES also should be obtained from the experimental flow field using the top-hat filter).

3.2 Forced isotropic turbulence

A statistically stationary isotropic turbulence is simulated using a 32^3 grid resolution. The main purpose of this simulation is to determine whether a low resolution LES using the LDKSGS model can reproduce the statistics (of the large scale structures) in a realistic, high Reynolds number turbulent field. The results are compared with the existing high resolution DNS data by Vincent and Meneguizzi (1991) and Jimenez *et al.* (1993) obtained at $Re_\lambda \approx 150$ and $Re_\lambda \approx 170$, respectively.

A statistically stationary turbulent field is obtained by forcing the large scales (i.e., the initial value of all Fourier modes with wave number components equal to 1 is kept fixed). The initial condition is obtained by generating a random realization of the energy spectrum (e.g., Briscolini and Santangelo, 1994),

$$E(k) = C\frac{k^4}{1+(k/k_0)^{5/3+4}} \qquad (11)$$

where $k_0 = 1$ and C is a constant which normalizes the initial total energy to be 0.5. In this study, LES are implemented under two different flow conditions. One is characterized by Taylor microscale Reynolds number $Re_\lambda \approx 260$, the integral scale Reynolds number $Re_\ell \approx 2400$, and the large-eddy turnover time $\tau \approx 3.7$; the other is characterized by $Re_\lambda \approx 80$, $Re_\ell \approx 220$, and $\tau \approx 4$ (here, those values are estimated in an approximate manner as described in Kim & Menon, 1995b). The simulations have been run for 27 and 25 large-eddy turnover times, respectively. To ensure statistical independence, 20 fields are used in statistical analysis for both cases (i.e., the time interval between successive fields is larger than (or at least same as) one large-eddy turnover time).

The temporal evolution of the mean turbulent kinetic energy is investigated (not shown here). After an initial decaying period, the mean turbulent kinetic energy remains at almost the same level, reflecting a balance between forcing at the large scales (the energy injection rate) and dissipation at the small scales (the energy dissipation rate). Only this energy equilibrium period of time is used in statistical analysis because it is closer to a statistically steady state.

Figure 3(a) shows the probability distribution of velocity differences, $\delta u(r) = u(x+r) - u(x)$, for various values of r (note that all values of r used here are comparable with the inertial range scales). For generality, δu is normalized so that $\sigma^2 = \langle \delta u^2 \rangle = 1$. The LES results (using the LDKSGS model at $Re_\lambda \approx 260$) clearly show that the distribution changes from a non-Gaussian (which has the wings) to a Gaussian, as r increases. The same behavior of the distribution was observed in the high resolution DNS of Vincent and Meneguizzi (1991). In addition to the basic agreement regarding the development of the non-Gaussian statistics, the LES accurately predicts the probability for each bin. Figure 3(b) shows an agreement between the distributions for $r = 0.39$ obtained from the LES and the DNS except for some deviation in the wing region. However, as is well known, the wings of the non-Gaussian distribution develop mainly due to small-scale fluctuations. Therefore, the deviation between the LES and the DNS results in the wings is somewhat natural; since in LES, most small scales are not resolved and even the resolved portion of small scales lies under strong influence of the top-hat filter implicitly implemented in the finite-difference code.

The statistics of velocity and its derivatives are also investigated. While the statistics of velocity are the property of the large scales which are mostly resolved in LES, the statistics of velocity derivative are the property of the dissipation range scales which are not resolved by LES. Therefore, the direct comparison of LES and DNS using the statistics of velocity derivative may be meaningless. A more useful comparison can be achieved by filtering the DNS field down to the same resolution as the LES. For the same grid resolution and flow conditions, the statistics of the LES and the filtered DNS should match well. However,

the velocity derivative statistics of the filtered DNS data are not available, therefore, the DNS statistics of velocity derivative obtained from the full resolution simulation (shown in the table 1) is being used only as a qualitative measure for the LES results. We computed the nth-order moments of the velocity and its derivative distributions using

$$S_n = \frac{\langle x^n \rangle}{\langle x^2 \rangle^{n/2}} \tag{12}$$

here, $\langle \cdot \rangle$ denotes ensemble-averaging. The results of this calculation is summarized in table 1. The results of the 512^3 DNS ($Re_\lambda \approx 170$), the 240^3 DNS ($Re_\lambda \approx 150$), and the 64^3 LES ($Re_\lambda \approx 140$) are obtained from Jimenez *et al.* (1993), Vincent and Meneguizzi (1991), and Briscolini and Santangelo (1994), respectively. (Note that different authors use a definition of Re_λ in different form, however, we use the original value provided by the authors without any correction.) The 64^3 LES was implemented using the Kraichnan's eddy viscosity where the small scales are parameterized reproducing a self-similar range of energy in spectral space. We simulated two different Reynolds number cases using the same grid resolution to investigate the effect of the Reynolds number on the statistics. As shown in the table, the velocity statistics appear not to depend on either the grid resolution or the Reynolds number simulated. However, the velocity derivative statistics were highly influenced by the grid resolution employed (it can be observed from the table that those values of the velocity derivative statistics are consistently decreased as the grid resolution becomes coarse from 512^3 to 32^3). In the LES, the effect of the Reynolds number on the velocity derivative statistics is not captured (in the DNS of Jimenez *et al.*, 1993, consistent increase in the velocity derivative statistics with Reynolds number increase was observed), since the velocity derivative statistics are strongly determined by the grid resolution employed.

Figures 4(a) and (b) show the temporal evolution of the model coefficient C_τ and the dissipation model coefficient C_ε (locally evaluated coefficients are volume-averaged for quantitative presentation). The LDKSGS model predicts $C_\tau \approx 0.056$ and $C_\varepsilon \approx 0.33$ for higher Reynolds number case ($Re_\lambda \approx 260$) and $C_\tau \approx 0.05$ and $C_\varepsilon \approx 0.44$ for lower Reynolds number case ($Re_\lambda \approx 80$). These values for C_τ are well matched with that suggested by Yoshizawa & Horiuti (1985); they recommended $C_\tau \approx 0.05$ from the framework of the two-scale direct-interaction approximation (TSDIA). (Note that, in the Reynolds-averaged turbulence models, a generally adopted value for C_τ is about 0.09; that is significantly larger than that for LES.) However, there are some discrepancies between C_ε values dynamically determined and suggested by Yoshizawa & Horiuti ($C_\varepsilon \approx 1$). From the observation of these figures, it can be roughly concluded that in LES of (forced) isotropic turbulence using the fixed grid resolution, a larger value of the model coefficient C_τ and a smaller value of the dissipation model coefficient C_ε is required as higher Reynolds number flows are simulated.

3.3 Turbulent mixing layer

Although it is generally accepted that turbulent mixing layers achieve self-similarity after initial development, there is still a lack of agreement (between different simulations or experiments) on the asymptotic growth rate and the turbulence properties in the self-similar period. The discrepancy becomes more severe in the numerical simulations (both DNS and LES) of temporally evolving turbulent mixing layers since the evolution of the flows is very sensitive to the initial state not only in the physical aspect but also in the numerical aspect. That is, the evolution of the flows varies greatly in simulations using different numerical schemes, grid resolutions and turbulent models, even though extremely accurate schemes and models are employed. Especially, since in LES, the SGS models are devised to predict the effect of the subgrid-scale turbulence on the large-scale turbulence, they are not capable of properly handling the artificial (somewhat unrealistic) turbulence prescribed in the initial field. Hence, the initial disturbance fields at different grid resolutions even obtained in a physically and a numerically consistent manner (such as by taking successive filtering to a full-resolution field) are recognized by the SGS model as being different initial states. This implies that the LES would fail to provide results which can be directly compared to the DNS data or the LES results at different resolutions. The only meaningful comparison of time accurate results can be achieved by a scaling using parameters which can remove the initial condition effects. This issue is addressed below.

Generally, turbulent mixing layers are considered self-similarly evolving if they grow linearly and the shapes of the mean velocity and turbulence profiles are independent of time (or location in spatially evolving mixing layers) when scaled by the time-dependent (or local in spatially evolving mixing layers) momentum thickness δ_m and the velocity difference ΔU. In temporally evolving mixing layers, the growth rate is generally scaled by the initial momentum thickness δ_m^0 and the velocity difference ΔU. This scaling is typically adopted only for the purpose of nondimensionalization, hence, time-accurate

evolution can be obscured by the effects of the initial conditions. To extract time-accurate information, the principal effects of initial development variability should be removed. This can be achieved by choosing appropriate scaling parameters in the self-similar period and using a reasonable reference point at the instant when self-similar evolution starts (i.e., when the mixing layer begins to grow linearly). However, both physically and numerically, it is difficult to precisely estimate this starting point of self-similarity. In the present study, this point is estimated by numerical investigation. First, the points where the first, second, and third derivatives of momentum thickness evolution curve have extreme (maximum and minimum) values, are sought. And then, these points are used as reference points for the momentum thickness growth rate scaling. It is found that the point where the second derivative of momentum thickness evolution curve has a maximum value, provides the most reliable time-accurate results. The present scaling can be described as follows,

$$\delta_m^*(t^*) = \frac{1}{\delta_m^S}\left[\delta_m(t^*) - \delta_m^S\right] \tag{13}$$

$$t^* = \frac{\Delta U}{\delta_m^S}\left(t - t^S\right) \tag{14}$$

where superscript $*$ denotes scaled variables and superscript S indicates the scaling parameters at the self-similarity starting point. Subtractions by δ_m^S and t^S are implemented to assign zero scaled time and scaled momentum thickness at the self-similarity starting point. This scaling is applied to both DNS and LES data of temporally evolving mixing layers and its capability in generating time-accurate results is demonstrated below.

Vreman *et al.* (1994b) simulated the temporal, weakly compressible (M=0.2) mixing layer in a cubic domain using 192^3 grid resolution. In their study, the length of the domain is $29.5\delta_\omega^0$ (where δ_ω^0 denotes the initial vorticity thickness) which is corresponding to four times the wavelength of the most unstable mode as predicted by linear stability theory at M=0.2. Periodic boundary conditions are imposed in the streamwise (x) and spanwise (z) directions, while in the cross-stream (y) direction the boundaries are assumed as slip walls. The initial velocity field is the hyperbolic-tangent profile, $u = \Delta U \tanh(2y/\delta_\omega^0)$, on which is superimposed a three-dimensional large-amplitude eigenfunction disturbance obtained from linear stability analysis (Sandham & Reynolds, 1991). For the present study of the temporally evolving incompressible mixing layer, the initial LES field is obtained by filtering the initial DNS field (generated using Vreman's code) for three different lengths of the domain, $28.3\delta_\omega^0$ (which corresponds to four times the wavelength of the most unstable mode as predicted by linear stability theory at M≃0), $50\delta_\omega^0$, and $100\delta_\omega^0$. Table 2 summarizes the test condition and the initial and self-similar starting point Reynolds number.

Figure 5(a) shows the evolution of the unscaled momentum thickness as a function of the unscaled time. According to the plot, all four simulations seem to evolve differently, hence, the direct comparison of the flow properties at the same (unscaled) time results poor agreement (not shown here). The scaling described in (13) and (14) is applied to these data and the results are plotted in figure 5(b). Now, curves for all three LES runs agree very well each other (the LDKSGS model seems to work consistently well for the relatively coarser, same resolutions but larger domain sizes, grids) but overpredict the growth rate over the DNS curve slightly. This difference between LES and DNS confirms the well-known fact that compressibility reduces mixing layer growth rate (Sandham & Reynolds, 1991). Figure 5(b) also includes the asymptotic growth rate (slope) obtained from the experiment of Bell and Mehta (1990) for a spatially evolving mixing layer begun from turbulent (tripped) splitter-plate boundary layers. The growth rates predicted by LES runs agree very well with the experiment.

The mean velocity profiles of the LES Run 2 at five times during the entire period after $t^* = 0$ are plotted with self-similar scaling using the time-dependent momentum thickness δ_m and the velocity difference ΔU in figure 6. Also included are the experimental data of Bell and Mehta (1990) (the experimental profiles have been shifted to center them at $y = 0$). The collapse of the data at the five times is excellent, and the mean profile agrees very well with the data of Bell and Mehta.

Figure 7 shows the Reynolds stress profile $\overline{uv}$ scaled using self-similar parameters at $t^* = 110$. The overall agreement between the DNS and the LES runs is quite good. Interestingly, the LES Runs 2 and 3 agree much better with the DNS than the LES Run 1, although their computational domain lengths computed using initial parameters agree less with that of DNS (see table 2). The poorer results of the LES Run 1 may stem from the fact that the computational domain of the LES Run 1 is not large enough to encompass the same structures resolved in the DNS at the chosen instant, even though both simulations start with the initially identical computational domain sizes. Therefore, from the above results, it can be concluded that the simulation parameters scaled by the self-similarity stating point parameters are more useful than those scaled by the initial

parameters especially for comparing time-accurate DNS/LES results.

Figures 8(a) and (b) show the evolution (with respect to the scaled time) of the model coefficient C_τ and the dissipation model coefficient C_ε computed from the LES Run 2. Averaging over the two homogeneous directions renders the coefficients as a function of time and the normal direction y. Five locations are chosen between the center plane ($y = 0\delta_m^S$) and the lower boundary plane ($y = -22.9\delta_m^S$). The volume-averaged coefficients are also included. At $t^* = 0$, both coefficients (especially, C_ε) computed on the center plane ($y = 0$) increase rapidly indicating that turbulence starts to decay by the viscous damping and realistic turbulence is about to develop. This fact confirms that the self-similarity starting point is accurately determined. The C_ε values computed on the planes other than the center plane ($y = 0$) are unphysically large during the initial period since the initial disturbances are applied to very thin layer around the center plane, however, these values rapidly decrease as the mixing layer grows.

4 Conclusions

In this paper, the LDKSGS model has been successfully applied to LES of high Reynolds number flows such as decaying and forced isotropic turbulence, and temporally evolving turbulent mixing layer. The capability of the LDKSGS model in predicting the energy decay rate has been demonstrated by simulating decaying isotropic turbulence and comparing the results to the experimental data (the LES results confirmed the power law decay which was observed in the experimental data). Furthermore, three different resolutions LES (at the coarsest resolution, about a half of the kinetic energy was not resolved) showed consistency in predicting the energy decay. This property of the LDKSGS model is very attractive, especially when the model is (to be) applied to complex and high Reynolds number flows where a significant amount of turbulent energy possibly lies in the unresolved scales. The application of the present model to forced (statistically stationary) isotropic turbulence also proves the capability of the LDKSGS model in reproducing the statistics (of the large scale structures) of a realistic, high Reynolds number turbulent field. The LES results, when compared to the high resolution DNS data, clearly show the accurate prediction of velocity statistics and the development of the non-Gaussian statistics (which was observed in the high resolution DNS). The capability of the LDKSGS model in predicting the time-accurate results has been further investigated by simulating the temporally-evolving turbulent mixing layer which is dominated by coherent structures and evolves from the linear stability regime up to a well developed turbulent flow field. Using the scaling which is capable of separating the distinct effects of initial development on the self-similar stage of the mixing layer evolution, it was demonstrated that the coarse grid simulations employing the LDKSGS model can provide time-accurate results which agree very well with existing direct numerical simulation and experimental data.

ACKNOWLEDGMENT

The authors wish to thank Professor B. Vreman for providing the initial disturbance field generator of turbulent mixing layer and the data presented in figures 5(b) and 7. This work is supported by the Fluid Dynamics Division of the Office of Naval Research under grant N00014-93-1-0342 (monitored by Dr. P. Purtell). This work was also supported in part by a grant of HPC time from the DoD HPC Centers: the Naval Oceanographic Office (NAVO) and the USAE Waterways Experiment Station (CEWES).

References

Bell, J. H. & Mehta, R. D. 1990 Development of a two-stream mixing layer from tripped and untripped boundary layers. *AIAA J.* **28**, 2034.

Briscolini, M. & Santangelo, P. 1994 The non-Gaussian statistics of the velocity field in low-resolution large-eddy simulations of homogeneous turbulence. *J. Fluid Mech.* **270**, 199.

Comte-Bellot, G. & Corsin, S. 1971 Simple Eulerian time correlation of full- and narrow-band velocity signals in grid-generated, 'isotropic' turbulence. *J. Fluid Mech.* **48**, 273.

Germano, M., Piomelli, U., Moin, P. & Cabot, W. H. 1991 A dynamic subgrid-scale eddy viscosity model. *Phys. Fluids* A **3**, 1760.

Ghosal, S., Lund, T. S., Moin, P. & Akselvoll, K. 1995 A dynamic localization model for large-eddy simulation of turbulent flows. *J. Fluid Mech.* **286**, 229.

Jimenez, J., Wray, A. A., Saffman, P. S. & Rogallo, R. S. 1993 The structure of intense vorticity in isotropic turbulence. *J. Fluid Mech.* **255**, 65.

Kim, W.-W. & Menon, S. 1995a A new dynamic one-equation subgrid-scale model for large eddy simulations. *AIAA Paper 95-0356, AIAA 33rd Aerospace Sciences Mtg, Reno, NV.*

Kim, W.-W. & Menon, S. 1995b On the properties of a localized dynamic subgrid-scale model for large-eddy simulations. Submitted to *J. Fluid Mech.*.

Lilly, D. K. 1992 A proposed modification of the Germano subgrid-scale closure method. *Phys. Fluids* **4**, 633.

Liu, S., Meneveau, C. & Katz, J. 1994 On the properties of similarity subgrid-scale models as deduced from measurements in a turbulent jet. *J. Fluid Mech.* **275**, 83.

Menon, S. & Yeung, P.-K. 1994 Analysis of subgrid models using direct and large-eddy simulations of isotropic turbulence. *Proc. AGARD 74th Fluid Dynamics Symp. on Application of Direct and Large Eddy Simulation to Transition and Turbulence, AGARD-CP-551*, p. 10-1.

Menon, S., Yeung, P.-K. & Kim, W.-W. 1995 Effect of subgrid models on the computed interscale energy transfer in isotropic turbulence. To appear in *Computers Fluids.*

Moin, P., Squires, K., Cabot, W. & Lee, S. 1991 A dynamic subgrid-scale model for compressible turbulence and scalar transport. *Phys. Fluids* A **3**, 2746.

Piomelli, U. 1993 High Reynolds number calculations using the dynamic subgrid-scale stress model. *Phys. Fluids* A **5**, 1484.

Sandham, N. D. & Reynolds, W. C. 1991 Three-dimensional simulations of large eddies in the compressible mixing layer. *J. Fluid Mech.* **224**, 133.

Squires, K. D. & Piomelli, U. 1994 Dynamic modeling of rotating turbulence. In *Turbulent shear flows 9* (ed. F. Durst, N. Kasagi, B. E. Launder, F. W. Schmidt & J. H. Whitelaw). Springer-Verlag, Heidelberg, p. 73.

Vincent, A. & Meneguzzi, M. 1991 The spatial structure and statistical properties of homogeneous turbulence. *J. Fluid Mech.* **225**, 1.

Vreman, B., Geurts, B. & Kuerten, H. 1994a Realizability conditions for the turbulent stress tensor in large-eddy simulation. *J. Fluid Mech.* **278**, 351.

Vreman, B., Geurts, B. & Kuerten, H. 1994b On the formulation of the dynamic mixed subgrid-scale model. *Phys. Fluids* **6**, 4057.

Yoshizawa, A. 1993 Bridging between eddy-viscosity-type and second-order models using a two-scale DIA. *Proc. 9th Symp. on Turbulent Shear Flows*, p. 23-1-1.

	u		$\partial u/\partial x$ ($\partial u/\partial y$)			
	S_4	S_6	S_3	S_4	S_5	S_6
512^3 DNS ($Re_\lambda \approx 170$)	2.80	12.5	-0.525	6.1 (9.4)	-12.0	125 (370)
240^3 DNS ($Re_\lambda \approx 150$)			-0.5 (-0.04)	5.9 (8.0)	-9	90
64^3 LES ($Re_\lambda \approx 140$)			-0.35 (0.06)	(4.5)		
32^3 LES ($Re_\lambda \approx 260$)	2.78	11.9	-0.32 (-0.01)	3.47 (4.87)	-3.48 (-0.11)	23.4 (49.9)
32^3 LES ($Re_\lambda \approx 80$)	2.80	12.1	-0.30 (0.03)	3.59 (4.93)	-3.57 (0.23)	25.8 (51.3)
Gaussian	3.0	15.0	0.0	3.0	0.0	15.0

Table 1. Higher-order moments for u-velocity and its gradients. The 512^3 DNS, 240^3 DNS, and 64^3 LES results are obtained from Jimenez *et al.* (1993), Vincent & Meneguizzi (1991), and Briscolini & Santangelo (1994), respectively.

	Domain size	$\Delta U \delta^S_{\omega\omega}/\nu$	$\Delta U \delta^0_{\omega\omega}/\nu$	$\Delta U \delta^0_{\omega}/\nu$
192^3 DNS	$55.9\delta^S_{\omega\omega}$ ($29.5\delta^0_{\omega}$)	106	79	200
LES Run 1	$39.5\delta^S_{\omega\omega}$ ($28.3\delta^0_{\omega}$)	143	78	200
LES Run 2	$45.7\delta^S_{\omega\omega}$ ($50\delta^0_{\omega}$)	219	113	200
LES Run 3	$49.8\delta^S_{\omega\omega}$ ($100\delta^0_{\omega}$)	402	201	200

Table 2. Temporally evolving mixing layer simulation parameters. The 192^3 DNS results is obtained from Vreman *et al.* (1994b).

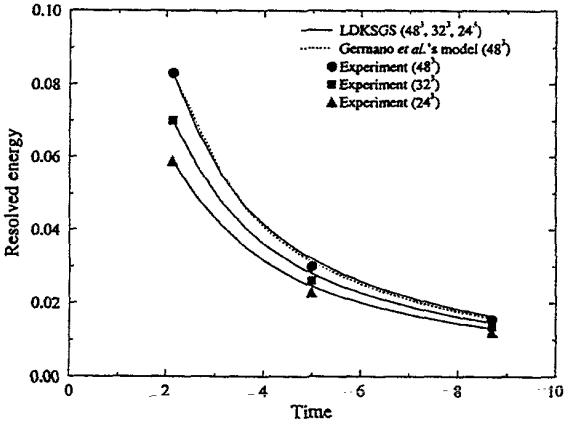

Figure 1. Decay of turbulent kinetic energy resolved in LES; compared to the experimental data by Comte-Bellot & Corsin (1971).

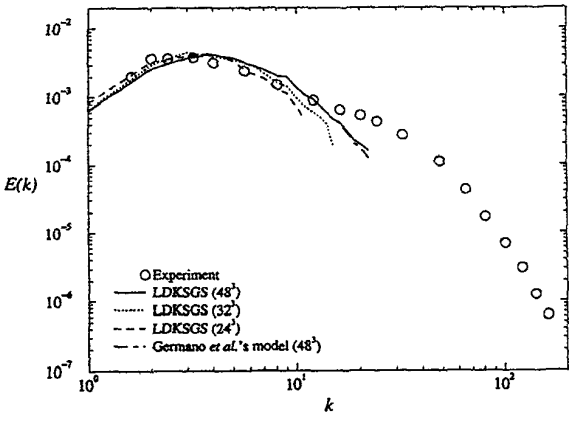

Figure 2(a). Energy spectra predicted by LES at $t^* = 4.98$; compared to the experimental data by Comte-Bellot & Corsin (1971).

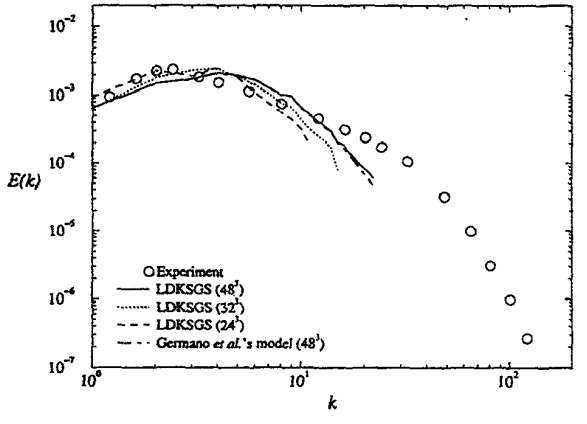

Figure 2(b). Energy spectra predicted by LES at $t^* = 8.69$; compared to the experimental data by Comte-Bellot & Corsin (1971).

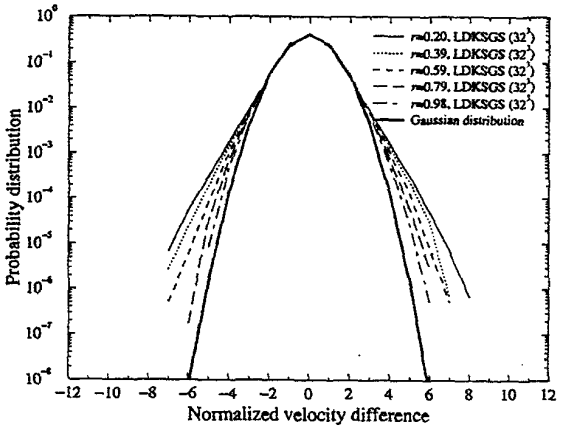

Figure 3(a). Probability distribution of normalized velocity difference for five different scales (r) predicted by 32^3 LES at $Re_\lambda = 260$.

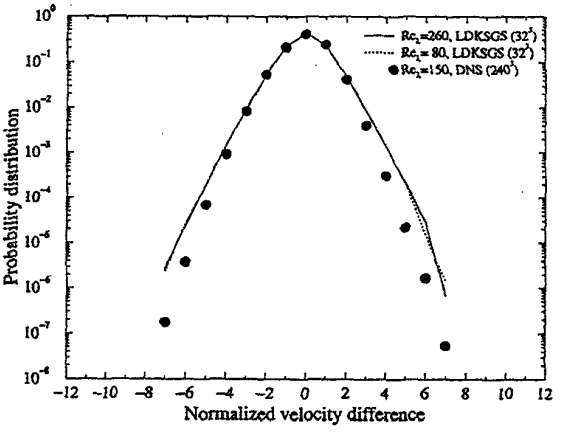

Figure 3(b). Probability distribution of normalized velocity difference for $r = 0.39$; compared to the DNS results by Vincent & Meneguizzi (1991).

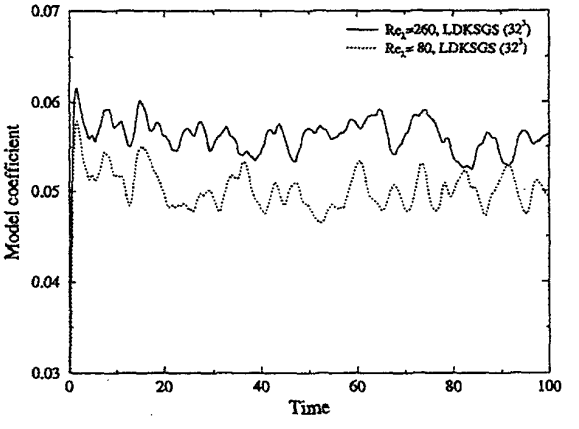

Figure 4(a). Time evolution of the model coefficients determined from 32^3 LES at two different Reynolds numbers.

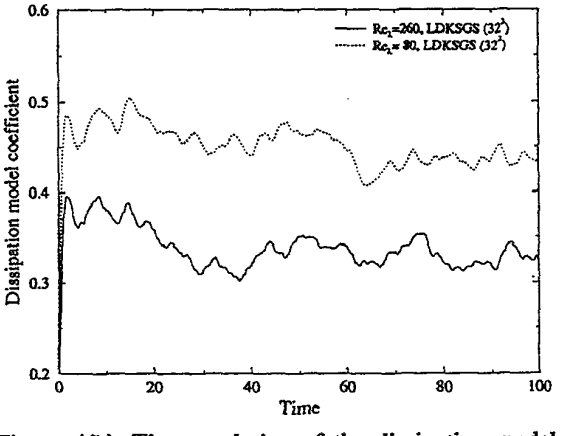

Figure 4(b). Time evolution of the dissipation model coefficients determined from 32^3 LES at two different Reynolds numbers.

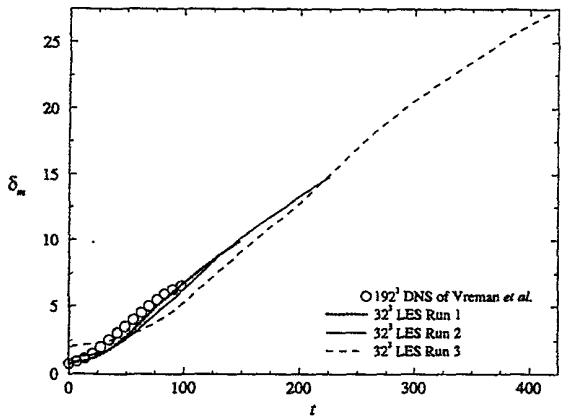

Figure 5(a). Time evolution of the momentum thickness in unscaled coordinates.

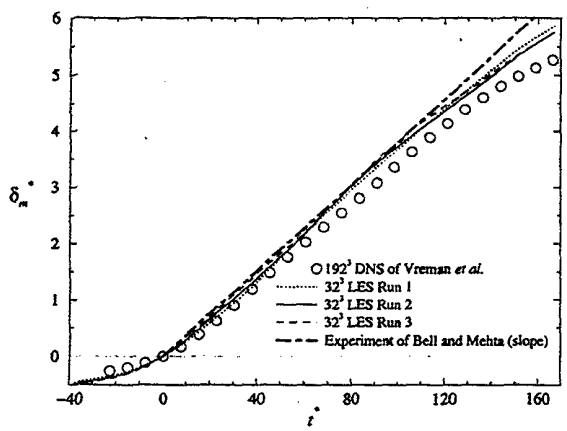

Figure 5(b). Time evolution of the momentum thickness in scaled coordinates using self-similarity starting parameters.

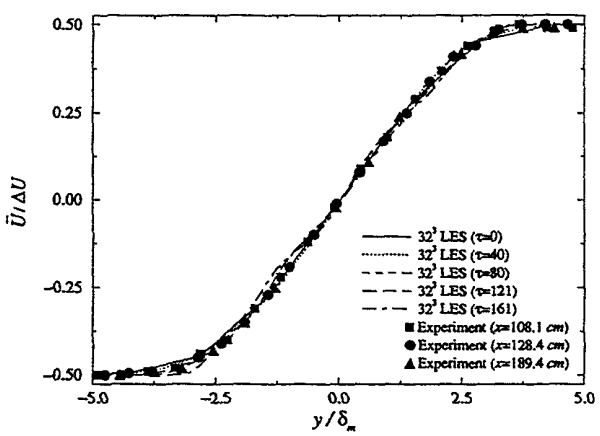

Figure 6. Mean streamwise velocity profiles in self-similar scaled coordinates compared with the experimental data of Bell and Mehta (1990).

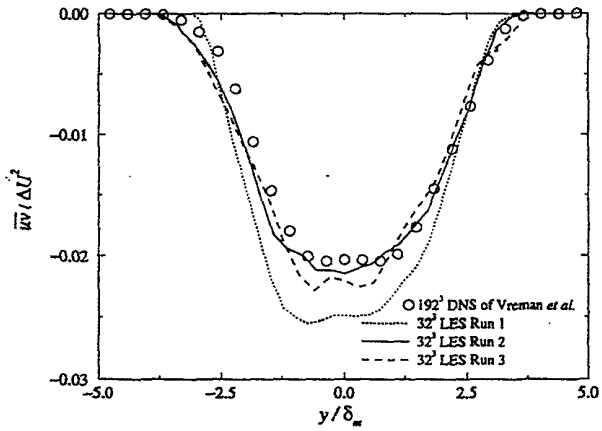

Figure 7. Comparison of the time-accurate simulation results in self-similar scaled coordinates for the Reynolds stress component $\overline{uv}$ at t^*=110.

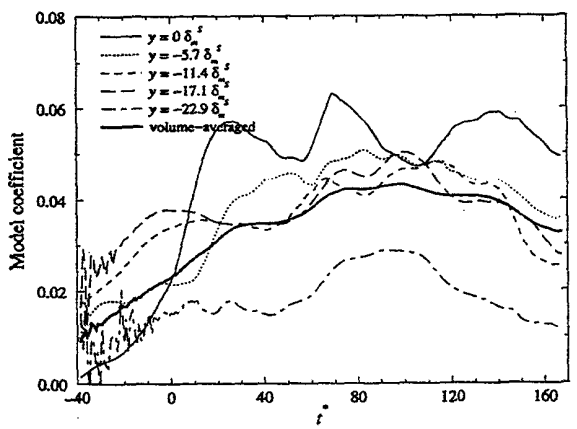

Figure 8(a). Time evolution of the plane-averaged model coefficients at five different locations along the normal direction.

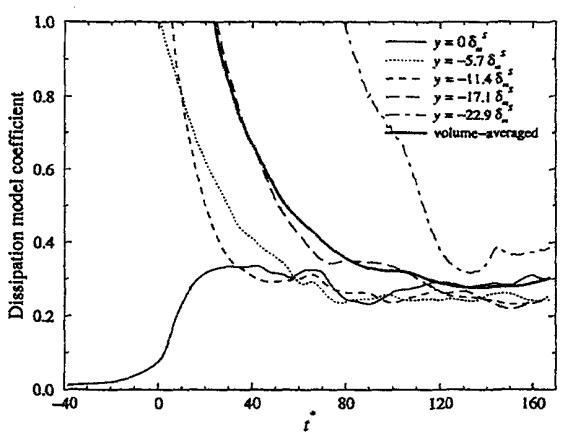

Figure 8(b). Time evolution of the plane-averaged dissipation model coefficients at five different locations along the normal direction.